J-RA 3 2 13006

Morphologic Edge Detection

James S. J. Lee
Robert M. Haralick
Linda G. Shapiro

Reprinted from
IEEE JOURNAL OF ROBOTICS AND AUTOMATION
Vol. RA-3, No. 2, April 1987

Morphologic Edge Detection

JAMES S. J. LEE, MEMBER, IEEE, ROBERT M. HARALICK, FELLOW, IEEE, AND LINDA G. SHAPIRO, SENIOR MEMBER, IEEE

Abstract—**Edge operators based on gray-scale morphologic operations are introduced. These operators can be efficiently implemented in near real time machine vision systems which have special hardware support for gray-scale morphologic operations. The simplest morphologic edge detectors are the dilation residue and erosion residue operators. The underlying motivation for these and some of their combinations are discussed and justified. Finally, the blur-minimum morphologic edge operator is defined. Its inherent noise sensitivity is less than the dilation or the erosion residue operators. Some experimental results are provided to show the validity of these morphologic operators. When compared with the enhancement/thresholding edge detectors and the cubic facet second derivative zero-crossing edge operator, the results show that all the edge operators have similar performance when the noise is small. However, as the noise increases, the second derivative zero-crossing edge operator and the blur-minimum morphologic edge operator have much better performance than the rest of the operators. The advantage of the blur-minimum edge operator is that it is less computationally complex than the facet edge operator.**

I. Introduction

EDGES in a scene are caused by changes in some physical properties of surfaces of the scene, such as illumination (shadows, for example), geometry (orientation or depth), and reflectance. As there is a direct relationship between the edges and the physical properties of a scene, much of the scene information can be recovered from an edge image. Thus edge detection is a key step in the early processing of a computer vision system. Edge detection converts a gray-scale image into a binary edge image which may have direction information. The transformation preserves a great deal of the useful information in the original image. The rest of the vision processes can deal with the simple form, instead of dealing with the gray-scale image directly.

One conventional approach to the problem of edge detection employs high spatial frequency enhancement/thresholding algorithms. These algorithms use spatial operators to enhance the original image, forming an edge enhancement strength map. A threshold is then applied to the edge strength map to determine the presence or absence of edge pixels.

The spatial operators can be differential operators or template matching operators (Rosenfeld and Kak [33]). Differential operators are typified by the Sobel edge operator (Duda *et al.* [4]). The template-matching operators include the Prewitt operator, the Kirsch operator, and the Robinson three-level and five-level operators. Both approaches are extremely widely used and are quite old in concept (see Prewitt [31], Kirsch [16], and Robinson [32]). However, most of the existing masks for these approaches appear rather ad hoc, and their theory is still being developed (for example, see Föglein [5]).

A number of edge detectors involve fitting a function to the image surface. They estimate edge locations from the best-fitting surface that approximates the real image surface. One of the earliest examples of this method was the Prewitt operator [31]. Another early work is the Hueckel detector [12], [13]. Brooks [2], Hummel [14], and Morgenthaler [26], [27] all use the surface fit concept in determining edges.

Haralick [7] proposed fitting the image with small planar surfaces or "facets." Edges are marked at pixels which belong to two such facets when the parameters of the two surfaces are inconsistent. The test for consistency is based on goodness of fit of each surface within its neighborhood, a χ^2 statistic. In subsequent work on edge detection, Haralick [9], [10] does a least squares fit to a bivariate cubic polynomial in the pixel's central neighborhood and determines directional derivatives from the fitting coefficients. Instead of computing an isotropic form of the second derivative, Haralick computes the second directional derivative in the direction of the gradient. If a pixel contains a high enough negatively sloped zero crossing of the second directional derivative taken in the direction of the gradient, the pixel is called an edge pixel.

Some recent edge detectors attempt to enhance edges by filtering. Modestino and Fries [22] suggested a procedure for detecting edges in noisy pictures using a Wiener filtering approach. Shanmugan *et al.* [35] proposed the use of an optimal two-dimensional linear operator for which the Laplacian of a Gaussian is an approximation. Marr and Hildreth [19] determined edges by first smoothing the image with a Gaussian filter and then taking the Laplacian of the resulting image.

A context dependent edge detection using a relaxation labeling scheme was proposed by Zucker *et al.* [40]. The general context approach is described in Haralick and Lee [11]. Montanari [23] and Martelli [20] proposed methods of linking together edge segments based on dynamic programming and heuristic search. Brenner *et al.* [41] implemented a boundary finding scheme for histopathology automation. The scheme is also based on heuristic search.

Mathematical morphology is an approach to image processing based on set theoretic concepts of shape. The early works include Dineen [3], Kirsch [15], Preston [28]–[30], Landsman *et al.* [15], Moore [24], [25], and Golay [6]. It was formalized at the Ecóle de Mines in Paris in the mid 1970's by Matheron [21], and extended by Serra [34] and Sternberg [36], [37]. It has grown to envelop a variety of applications and hardwares.

Manuscript received November 18, 1985; revised August 7, 1986.

J. S. J. Lee was with Machine Vision International, Ann Arbor, MI. He is now with Boeing High Tech Center, P.O. Box 24969, MS 7J-24, Seattle, WA 98124-6269, USA.

R. M. Haralick and L. G. Shapiro were with Machine Vision International, Ann Arbor, MI. They are now with the Department of Electrical Engineering, University of Washington, Seattle, WA 98105, USA.

IEEE Log Number 8613006.

0882-4967/87/0400-0142$01.00 © 1987 IEEE

Several companies manufacturing machine vision hardware successfully use mathematical morphology to solve industrial machine vision problems (MVI) [18]. The machines they produce can deal with morphological operations more efficiently than other operations. Judging by the scientific archival literature, the techniques of mathematical morphology seem to be less used and less explored by the academic research communities.

This paper explores the use of gray-scale morphology in edge detection. Despite their computational simplicity and effectiveness, we are not aware of any gray-scale morphologic edge detectors discussed in the image processing literature.

In the next section, we define some of the basic morphologic operations. In Section III, we introduce the simplest morphologic edge operators and explain their performance. We then introduce different combinations of the simple operators. Section IV discusses some improved morphologic edge operators. Section V provides some experimental results of the morphologic edge operators and of comparisons with the cubic facet edge detector (Haralick [10]) and the enhancement/thresholding edge operators.

II. Basic Morphologic Operations

An image can be represented by a set of pixels. The morphologic operators work with two images: the original data to be analyzed and a structuring element, which is analogous to the kernel of a convolution operation. Each structuring element has a shape which can be thought of as a parameter to the operation.

First we consider the case of binary images. Let A be the set of points representing the binary one pixels of the original binary image and B be the set of points representing the binary one pixels of a structuring element. The *dilation* of A by B, denoted $A \oplus B$, is defined by

$$A \oplus B = \bigcup_{a \in A} \{b+a \mid b \in B\}. \tag{1}$$

The *erosion* of A by B, denoted $A \ominus B$, is defined by

$$A \ominus B = \{p \mid B+p \subseteq A\}. \tag{2}$$

The extensions of the morphologic transformations from binary into gray-scale processing by Sternberg [36]–[39] in the mid 1980's introduced a natural morphologic generalization of the dilation and erosion operations.

The dilation of a gray-scale image f by a gray-scale structuring element b is denoted by d and is defined by

$$d(r, c) = \max_{i,j} \; (f(r-i, c-j) + b(i, j)) \tag{3}$$

where the maximum is taken over all (i, j) in the domain of b such that $(r - i, c - j)$ is in the domain of f. The domain of d is the dilation of the domain of f with the domain of b. The erosion of a gray-scale image f by a structuring element b is denoted by e and is defined by

$$e(r, c) = \min_{i,j} \; (f(r+i, c+j) - b(i, j)) \tag{4}$$

where the minimum is taken over all (i, j) in the domain of b. The domain of e is the domain of f eroded by the domain of b.

The algorithms of mathematical morphology combine sequences of dilations and erosions, and their residues. These operations often produce useful and pleasantly surprising results.

III. Understanding the Simple Morphologic Edge Detectors

The purpose of this section is to explore some simple morphologic edge detectors which do not work well to provide some understanding of morphologic operators and to provide the basis for those discussed in Section IV which do work well. A simple method of performing gray-scale edge detection in a morphology-based vision system is to take the difference between an image and its erosion by a small rod-shaped structuring element. The difference image is the image of edge strength. We can then select an appropriate threshold value to threshold the edge strength image into a binary edge image.

We denote the center of a local neighborhood by (0, 0) and a point which is a distance δr from the center in row direction and a distance δc from the center in column direction by $(\delta r, \delta c)$. We define the rod as a gray-scale structuring element which is flat on top and has a disk-shaped domain. As an example, the domain of the structuring element rod of radius 1 is defined by the set

$$D_{\text{rod 1}} = \{(0, -1), (0, 1), (-1, 0), (1, 0)\}.$$

Let $b: D_{\text{rod1}} \rightarrow \{0, \cdots, 255\}$ be the rod 1 structuring element. Since a rod is flat on top, the gray-scale value of all the $b(r, c)$, $(r, c) \in D_{\text{rod 1}}$, is zero.

The erosion of a gray-scale image $f(r, c)$ by the structuring element rod of radius 1 can be carried out by the rule:

$$e(r, c) = \min_{(i,j) \in D_{\text{rod 1}}} [f(r+i, c+j) - b(r, c)] \tag{5}$$

which in the case of a zero height structuring element becomes

$$e(r, c) = \min_{(i,j) \in D_{\text{rod 1}}} [f(r+i, c+j)]. \tag{6}$$

The erosion residue edge detector produces the edge strength image G_e defined by

$$\begin{aligned} G_e(r, c) &= f(r, c) - e(r, c) \\ &= f(r, c) - \min_{(i,j) \in D_{\text{rod 1}}} f(r+i, c+j) \\ &= \max_{(i,j) \in D_{\text{rod 1}}} [f(r, c) - f(r+i, c+j)]. \end{aligned} \tag{7}$$

Since $D_{\text{rod 1}}$ includes exactly the four connected neighbors of position (0, 0), the edge strength image we obtain is

$$G_e(r, c) = \max_{(i,j) \in N_4(r,c)} [f(r, c) - f(i, j)] \tag{8}$$

where $N_4(r, c)$ is the set of four connected neighbors of position (r, c).

We can now interpret the morphologic edge operator as a local neighborhood nonlinear operator which takes the maxi-

mum among the four first differences in directions 0°, 90°, 180°, and 270°.

A natural nonmorphological variation of this operator takes the summation instead of maximization. This is the negative of the familiar linear digital Laplacian operator $\nabla^2 f(r, c)$ (Rosenfeld [33]) which is the digital convolution of $f(r, c)$ with the kernel

$$\begin{matrix} 0 & -1 & 0 \\ -1 & 4 & -1 \\ 0 & -1 & 0. \end{matrix}$$

To compare the performance of the nonlinear morphological edge operator with the linear Laplacian operator, we apply them to four perfect digital step edge patterns of edge contrast E running in directions 0°, 90°, 45°, and 135°, respectively, as

$$\begin{matrix} E\ E\ E & E\ E\ 0 & E\ E\ E & E\ E\ E \\ E\ E\ E & E\ E\ 0 & E\ E\ 0 & 0\ E\ E \\ 0\ 0\ 0 & E\ E\ 0 & E\ 0\ 0 & 0\ 0\ E. \\ E_{0°} & E_{90°} & E_{45°} & E_{135°} \end{matrix}$$

The magnitude of the responses of G and $\nabla^2 f$ are as follows:

$$\begin{matrix} & E_{0°} & E_{90°} & E_{45°} & E_{135°} \\ G_e & E & E & E & E \\ \nabla^2 f & E & E & 2E & 2E\ . \end{matrix}$$

Thus the responses of $\nabla^2 f$ to these edges are E, E, $2E$, and $2E$, a bias of two in favor of the diagonal edges. These biases are eliminated if we use the morphological operator G_e instead of $\nabla^2 f$. G_e yields values in the same range as the original gray-scale values, which is most convenient on any computer vision system that has frame buffer limitations on the range of gray-scale values.

Next we try both operators on a single noise point pattern with noise height h:

$$\begin{matrix} 0 & 0 & 0 \\ 0 & h & 0\ . \\ 0 & 0 & 0 \end{matrix}$$

The responses of G_e and $\nabla^2 f$ are h and $4h$, respectively. Thus although both G_e and $\nabla^2 f$ are noise sensitive, the noise response of $\nabla^2 f$ is four times the response of G_e and hence four times the response of $\nabla^2 f$ on a vertical or horizontal ideal step edge with edge contrast h.

It is also possible to increase the neighborhood size of the morphologic edge operator by increasing the size of the structuring element used on the erosion operation. For example, we can have an eight-connected neighborhood edge operator by changing the structuring element to be flat on top and have domain

$$D_{8-\text{connected}} = \{(-1, -1), (0, -1), (1, -1), (-1, 0), (1, 0), (-1, 1), (0, 1), (1, 1)\}. \quad (9)$$

The edge strength image we obtain is then

$$G_{e8-\text{connected}}(r, c) = \max_{(i,j) \in N_8(r,c)} [f(r, c) - f(i, j)] \quad (10)$$

where $N_8(r, c)$ is the set of eight connected neighbors of image position (r, c).

The corresponding linear Laplacian operator which has eight connected neighborhood support can be implemented as the digital convolution of $f(r, c)$ with the kernel

$$\begin{matrix} -1 & -1 & -1 \\ -1 & 8 & -1\ . \\ -1 & -1 & -1 \end{matrix}$$

We now apply both operators to the four perfect digital step edge patterns $E_{0°}$, $E_{90°}$, $E_{45°}$, and $E_{135°}$. The magnitude of the responses of G_e and $\nabla^2 f$ are as follows:

$$\begin{matrix} & E_{0°} & E_{90°} & E_{45°} & E_{135°} \\ G_{e8-\text{connected}} & E & E & E & E \\ \nabla^2 f_{8-\text{connected}} & 3E & 3E & 3E & 3E. \end{matrix}$$

With increased neighborhood size, the $\nabla^2 f$ operator achieves uniform performance on these edges. The response of both operators on the single noise point pattern are h and $8h$, respectively. Thus both operators are noise sensitive, the Laplacian being more noise sensitive. This explains why the raw Laplacian operator is not a good edge detector in noisy images.

It is now common to filter noisy images by a Gaussian filter and then apply a Laplacian operator. Edges are located at zero-crossings of the Laplacian (Marr and Hildreth [19]). However, the Gaussian filter can shift the positions of most of the edges in real images.

The erosion residue morphological edge detector is a nonlinear Laplacian-like operator which is also noise sensitive; it cannot be a good edge detector for noisy images. The rule that increasing the neighborhood size of the operator will reduce the amount of noise fails with the erosion residue morphological edge detector. Consider, for example, the erosion residue morphological edge detector on the following image pattern

$$\begin{matrix} F\ F\ F\ F\ F \\ F\ F\ F\ F\ F \\ F\ F\ 0\ F\ F\ . \\ F\ F\ F\ F\ F \\ F\ F\ F\ F\ F \end{matrix}$$

The pattern shown above is a flat area with pixel intensity F and a noise spike at the center of this area with pixel intensity zero. The response of the morphological edge operator is

$$\begin{matrix} 0\ 0\ 0\ 0\ 0 \\ 0\ F\ F\ F\ 0 \\ 0\ F\ 0\ F\ 0 \\ 0\ F\ F\ F\ 0 \\ 0\ 0\ 0\ 0\ 0 \end{matrix}$$

which has the same value F for each of the eight-connected neighbors of the center point. If we increase the size of the neighborhood support of the morphological operator, the number of pixels which are assigned the value F will also increase accordingly. As a matter of fact, each pixel of the

neighborhood support except the center point will be assigned the value F. Thus a larger neighborhood can result in worse results with this operator.

The erosion residue morphological edge detector is position biased. It only gives edge strength to border pixels on that side of the edge where the pixels have the higher value. For example, the operator only gives the inside boundary of the higher valued checkers of a perfect checkerboard image its corresponding edge strength and gives the outside boundary of the higher valued checkers edge strength zero.

To resolve this bias and give both inside and outside boundaries of the checkers their corresponding edge strengths, the dilation residue morphological edge detector can be used in conjunction with the erosion residue operator. The dilation residue operator takes the difference between a dilated image and its original image. For example, if the structuring element for the dilation is a rod of radius 1, then the dilation of the gray-scale image $f(r, c)$ is

$$d(r, c) = \max_{(i,j)\in D_{\text{rod 1}}} [f(r-i, c-j)] \tag{11}$$

and the edge strength image is

$$\begin{aligned} G_d(r, c) &= d(r, c) - f(r, c) \\ &= \max_{(i,j)\in N_4(x,y)} [f(i, j) - f(r, c)]. \end{aligned} \tag{12}$$

It is obvious that this operator only gives edge strength to that side of the edge which has the lower value.

A position unbiased edge operator can be obtained by a combination of the operators $G_e(r, c)$ and $G_d(r, c)$ using the pixelwise minimum, maximum, or sum. Let us consider the maximum first. Define

$$\begin{aligned} E(r, c) &= \max\,(G_e(r, c), G_d(r, c)) \\ &= \max_{(i,j)\in N(r, c)} |f(r, c) - f(i, j)| \end{aligned} \tag{13}$$

where $N(r, c)$ is the neighborhood support of the structuring element for both dilation and erosion operations.

To understand the performance of this operator, we apply it on four perfect digital step edge patterns of edge contrast E, one ideal ramp edge pattern of edge contrast E, and one single noise pattern of noise height N, as follows:

$$\begin{matrix} E\ E\ E\ E\ E \\ E\ E\ E\ E\ E \\ E\ E\ E\ E\ E \\ 0\ 0\ 0\ 0\ 0 \\ 0\ 0\ 0\ 0\ 0 \end{matrix} \qquad \begin{matrix} E\ E\ E\ 0\ 0 \\ E\ E\ E\ 0\ 0 \\ E\ E\ E\ 0\ 0 \\ E\ E\ E\ 0\ 0 \\ E\ E\ E\ 0\ 0 \end{matrix}$$

$E_{0°}$ $E_{90°}$

$$\begin{matrix} E\ E\ E\ E\ E \\ E\ E\ E\ E\ 0 \\ E\ E\ E\ 0\ 0 \\ E\ E\ 0\ 0\ 0 \\ E\ 0\ 0\ 0\ 0 \end{matrix} \qquad \begin{matrix} E\ E\ E\ E\ E \\ 0\ E\ E\ E\ E \\ 0\ 0\ E\ E\ E \\ 0\ 0\ 0\ E\ E \\ 0\ 0\ 0\ 0\ E \end{matrix}$$

$E_{45°}$ $E_{135°}$

$$\begin{matrix} 0\ 0\ E/2\ E\ E \\ 0\ 0\ E/2\ E\ E \\ 0\ 0\ E/2\ E\ E \\ 0\ 0\ E/2\ E\ E \\ 0\ 0\ E/2\ E\ E \end{matrix} \qquad \begin{matrix} 0\ 0\ 0\ 0\ 0 \\ 0\ 0\ 0\ 0\ 0 \\ 0\ 0\ N\ 0\ 0 \\ 0\ 0\ 0\ 0\ 0 \\ 0\ 0\ 0\ 0\ 0 \end{matrix}$$

$E_{r0°}$ noise

The results of this edge operator when the neighborhood support is $N_4(r, c)$ are

$$\begin{matrix} 0\ 0\ 0\ 0\ 0 \\ 0\ 0\ 0\ 0\ 0 \\ E\ E\ E\ E\ E \\ E\ E\ E\ E\ E \\ 0\ 0\ 0\ 0\ 0 \end{matrix} \qquad \begin{matrix} 0\ 0\ E\ E\ 0 \\ 0\ 0\ E\ E\ 0 \\ 0\ 0\ E\ E\ 0 \\ 0\ 0\ E\ E\ 0 \\ 0\ 0\ E\ E\ 0 \end{matrix}$$

$E_{0°}$ $E_{90°}$

$$\begin{matrix} 0\ 0\ 0\ 0\ E \\ 0\ 0\ 0\ E\ E \\ 0\ 0\ E\ E\ 0 \\ 0\ E\ E\ 0\ 0 \\ E\ E\ 0\ 0\ 0 \end{matrix} \qquad \begin{matrix} E\ 0\ 0\ 0\ 0 \\ E\ E\ 0\ 0\ 0 \\ 0\ E\ E\ 0\ 0 \\ 0\ 0\ E\ E\ 0 \\ 0\ 0\ 0\ E\ E \end{matrix}$$

$E_{45°}$ $E_{135°}$

$$\begin{matrix} 0\ E/2\ E/2\ E/2\ 0 \\ 0\ E/2\ E/2\ E/2\ 0 \\ 0\ E/2\ E/2\ E/2\ 0 \\ 0\ E/2\ E/2\ E/2\ 0 \\ 0\ E/2\ E/2\ E/2\ 0 \end{matrix} \qquad \begin{matrix} 0\ 0\ 0\ 0\ 0 \\ 0\ 0\ N\ 0\ 0 \\ 0\ N\ N\ N\ 0 \\ 0\ 0\ N\ 0\ 0 \\ 0\ 0\ 0\ 0\ 0 \end{matrix}$$

$E_{r0°}$ noise

Now the performance of the edge operator can be easily evaluated. This operator performs perfectly on ideal step edge patterns. However, it is sensitive to noise. It responds with five noise edge points to a single noise point. The results are even worse for the ideal ramp edge pattern. The detected edge pattern for the ramp should have a single pixel width edge line, and its edge strength should be equal to the edge contrast. Instead, this operator assigns edge strength of only half the edge contrast, and the detected edge is wide, three pixels in width.

We now consider the edge operator which is defined as the summation of $G_e(r, c)$ and $G_d(r, c)$. Thus

$$E(r, c) = G_e(r, c) + G_d(r, c). \tag{14}$$

To see the performance of this operator, we apply it on the edge patterns we used to test the maximum version edge operator. The results of this edge operator when the neighborhood support for dilation and erosion is $N_4(r, c)$ are

$$\begin{matrix} 0\ 0\ 0\ 0\ 0 \\ 0\ 0\ 0\ 0\ 0 \\ E\ E\ E\ E\ E \\ E\ E\ E\ E\ E \\ 0\ 0\ 0\ 0\ 0 \end{matrix} \qquad \begin{matrix} 0\ 0\ E\ E\ 0 \\ 0\ 0\ E\ E\ 0 \\ 0\ 0\ E\ E\ 0 \\ 0\ 0\ E\ E\ 0 \\ 0\ 0\ E\ E\ 0 \end{matrix}$$

$E_{0°}$ $E_{90°}$

$$\begin{matrix} 0&0&0&0&E \\ 0&0&0&E&E \\ 0&0&E&E&0 \\ 0&E&E&0&0 \\ E&E&0&0&0 \end{matrix} \qquad \begin{matrix} E&0&0&0&0 \\ E&E&0&0&0 \\ 0&E&E&0&0 \\ 0&0&E&E&0 \\ 0&0&0&E&E \end{matrix}$$

$E_{45°}$ $E_{135°}$

$$\begin{matrix} 0&E/2&E&E/2&0 \\ 0&E/2&E&E/2&0 \\ 0&E/2&E&E/2&0 \\ 0&E/2&E&E/2&0 \\ 0&E/2&E&E/2&0 \end{matrix} \qquad \begin{matrix} 0&0&0&0&0 \\ 0&0&N&0&0 \\ 0&N&N&N&0 \\ 0&0&N&0&0 \\ 0&0&0&0&0 \end{matrix}$$

$E_{r0°}$ noise

It is easy to see that, like the maximum version of this edge operator, the summation version performs perfectly on ideal step edge patterns and is also noise sensitive. It responds with five noise edge points to a single noise point. However, for the ideal ramp edge pattern, it detects an edge line whose edge strength equals edge contrast and two lines on both sides of the edge line whose edge strength equals half-edge contrast. Thus, by thresholding with a value greater than half-edge contrast, it is possible to have perfect performance on the ideal ramp edge pattern in the sense that it detects a single width edge line.

Finally, we consider the edge operator which is defined as the minimum of $G_e(r, c)$ and $G_d(r, c)$. Hence

$$E(r, c) = \min \{G_e(r, c), G_d(r, c)\}. \tag{15}$$

To understand the performance of this operator, we again apply it on the edge patterns we used to test the maximum and summation version edge operators. The results of this edge operator when the neighborhood support for dilation and erosion is $N_4(r, c)$ are

$$\begin{matrix} 0&0&0&0&0 \\ 0&0&0&0&0 \\ 0&0&0&0&0 \\ 0&0&0&0&0 \\ 0&0&0&0&0 \end{matrix} \qquad \begin{matrix} 0&0&0&0&0 \\ 0&0&0&0&0 \\ 0&0&0&0&0 \\ 0&0&0&0&0 \\ 0&0&0&0&0 \end{matrix}$$

$E_{0°}$ $E_{90°}$

$$\begin{matrix} 0&0&0&0&E \\ 0&0&0&0&0 \\ 0&0&0&0&0 \\ 0&0&0&0&0 \\ 0&0&0&0&0 \end{matrix} \qquad \begin{matrix} 0&0&0&0&0 \\ 0&0&0&0&0 \\ 0&0&0&0&0 \\ 0&0&0&0&0 \\ 0&0&0&0&0 \end{matrix}$$

$E_{45°}$ $E_{135°}$

$$\begin{matrix} 0&0&E/2&0&0 \\ 0&0&E/2&0&0 \\ 0&0&E/2&0&0 \\ 0&0&E/2&0&0 \\ 0&0&E/2&0&0 \end{matrix} \qquad \begin{matrix} 0&0&0&0&0 \\ 0&0&0&0&0 \\ 0&0&0&0&0 \\ 0&0&0&0&0 \\ 0&0&0&0&0 \end{matrix}$$

$E_{r0°}$ noise

The results of this operator are interesting. The performance on the ideal ramp edge pattern is promising. The operator can detect a single edge line with edge strength $E/2$, and it is noise insensitive. It has no response when applied to the single noise point. Unfortunately, it is not able to detect ideal step edge patterns. This motivates a new edge operator which first performs a blur operation to convert all the ideal step edges into ideal ramp edges and then applies the minimum version of the edge operator to them. In the next section, we will analyze this blur-minimum operator and some variations in greater detail.

IV. Effective Morphologic Edge Operators

As shown in the previous section, the simple morphological edge operators based on erosion or dilation residues are either sensitive to noise or cannot detect ideal step edges. In this section we discuss some effective morphological edge operators which can detect ideal step edges and are not noise sensitive. They are the improved dilation and erosion residue operators and the blur-minimum operator.

A. Improved Residue Operators

1) Improved Dilation Residue Operator: In this section we introduce an improved version of the dilation residue operator $G_d(r, c)$. Let a_1, a_2, a_3, a_4, and D_2 be structuring elements which are flat on top. Let the domains of these structuring elements be given by

$$D_{a1} = \{(-1, 0), (0, 1)\}$$

$$D_{a2} = \{(0, -1), (1, 0)\}$$

$$D_{a3} = \{(-1, 0), (0, -1)\}$$

$$D_{a4} = \{(0, 1), (1, 0)\}$$

$$D_2 = \{(-1, -1), (-1, 1), (1, -1), (1, 1)\}. \tag{16}$$

The operator is defined by

$$G'_d(r, c) = \min \{\text{dilation}_{D_{\text{rod }1}}(r, c) - f(r, c), \text{dilation}_{D_2}(r, c) - f(r, c), G''_d(r, c)\} \tag{17}$$

where $G''_d(r, c)$ is defined by

$$G''_d(r, c) = \max \{|(\text{dilation}_{a1}(r, c) - f(r, c)) - (\text{dilation}_{a2}(r, c) - f(r, c))|, |(\text{dilation}_{a3}(r, c) - f(r, c)) - (\text{dilation}_{a4}(r, c) - f(r, c))|\}. \tag{18}$$

To see the performance of this operator, we apply it on four perfect digital step edge patterns of edge contrast E, one ideal ramp edge pattern of edge contrast E, and two single noise patterns of noise height N:

$$\begin{matrix} E&E&E&E&E \\ E&E&E&E&E \\ E&E&E&E&E \\ 0&0&0&0&0 \\ 0&0&0&0&0 \end{matrix} \qquad \begin{matrix} E&E&E&0&0 \\ E&E&E&0&0 \\ E&E&E&0&0 \\ E&E&E&0&0 \\ E&E&E&0&0 \end{matrix}$$

$E_{0°}$ $E_{90°}$

$$\begin{matrix} E & E & E & E & E \\ E & E & E & E & 0 \\ E & E & E & 0 & 0 \\ E & E & 0 & 0 & 0 \\ E & 0 & 0 & 0 & 0 \end{matrix} \qquad \begin{matrix} E & E & E & E & E \\ 0 & E & E & E & E \\ 0 & 0 & E & E & E \\ 0 & 0 & 0 & E & E \\ 0 & 0 & 0 & 0 & E \end{matrix}$$

$E_{45°}$ $E_{135°}$

$$\begin{matrix} 0 & 0 & E/2 & E & E \\ 0 & 0 & E/2 & E & E \\ 0 & 0 & E/2 & E & E \\ 0 & 0 & E/2 & E & E \\ 0 & 0 & E/2 & E & E \end{matrix} \qquad \begin{matrix} 0 & 0 & 0 & 0 & 0 \\ 0 & 0 & 0 & 0 & 0 \\ 0 & 0 & N & 0 & 0 \\ 0 & 0 & 0 & 0 & 0 \\ 0 & 0 & 0 & 0 & 0 \end{matrix}$$

$E_{r0°}$ noise 1

$$\begin{matrix} N & N & N & N & N \\ N & N & N & N & N \\ N & N & 0 & N & N \\ N & N & N & N & N \\ N & N & N & N & N \end{matrix}.$$

noise 2

The results of $G_d'(r, c)$ are

$$\begin{matrix} 0 & 0 & 0 & 0 & 0 \\ 0 & 0 & 0 & 0 & 0 \\ 0 & 0 & 0 & 0 & 0 \\ E & E & E & E & E \\ 0 & 0 & 0 & 0 & 0 \end{matrix} \qquad \begin{matrix} 0 & 0 & 0 & E & 0 \\ 0 & 0 & 0 & E & 0 \\ 0 & 0 & 0 & E & 0 \\ 0 & 0 & 0 & E & 0 \\ 0 & 0 & 0 & E & 0 \end{matrix}$$

$E_{0°}$ $E_{90°}$

$$\begin{matrix} 0 & 0 & 0 & 0 & 0 \\ 0 & 0 & 0 & 0 & E \\ 0 & 0 & 0 & E & 0 \\ 0 & 0 & E & 0 & 0 \\ 0 & E & 0 & 0 & 0 \end{matrix} \qquad \begin{matrix} 0 & 0 & 0 & 0 & 0 \\ E & 0 & 0 & 0 & 0 \\ 0 & E & 0 & 0 & 0 \\ 0 & 0 & E & 0 & 0 \\ 0 & 0 & 0 & E & 0 \end{matrix}$$

$E_{45°}$ $E_{135°}$

$$\begin{matrix} 0 & E/2 & E/2 & 0 & 0 \\ 0 & E/2 & E/2 & 0 & 0 \\ 0 & E/2 & E/2 & 0 & 0 \\ 0 & E/2 & E/2 & 0 & 0 \\ 0 & E/2 & E/2 & 0 & 0 \end{matrix} \qquad \begin{matrix} 0 & 0 & 0 & 0 & 0 \\ 0 & 0 & 0 & 0 & 0 \\ 0 & 0 & 0 & 0 & 0 \\ 0 & 0 & 0 & 0 & 0 \\ 0 & 0 & 0 & 0 & 0 \end{matrix}$$

$E_{r0°}$ noise 1

$$\begin{matrix} 0 & 0 & 0 & 0 & 0 \\ 0 & 0 & 0 & 0 & 0 \\ 0 & 0 & 0 & 0 & 0 \\ 0 & 0 & 0 & 0 & 0 \\ 0 & 0 & 0 & 0 & 0 \end{matrix}.$$

noise 2

Thus, like the simple dilation residue operator, this operator assigns edge strength E to all the edge pixels which are on the low value side of the ideal step edge, and it detects two edge lines of half-edge contrast from ideal ramp edge patterns. However, unlike the simple dilation residue operator, it will not pick up a noise pixel. Hence this is an improved version of the $G_d(r, c)$ operator. It is also noted that this operator does not need any blurring as preprocessing.

2) Improved Erosion Residue Operator: In this section we introduce an improved version of the erosion residue operator $G_e(r, c)$. Let a_1, a_2, a_3, a_4, and D_2 be the structuring elements which were defined in the previous section. Then the improved erosion residue operator is defined by

$$G_e'(r, c) = \min \{f(r, c) - \text{erosion}_{D_{\text{rod}\,1}}(r, c), f(r, c) - \text{erosion}_{D_2}(r, c), G_e''(r, c)\} \quad (19)$$

where $G_e''(r, c)$ is defined as

$$\begin{aligned} G_e''(r, c) = \max \{ & |(f(r, c) - \text{erosion}_{a1}(r, c)) \\ & - (f(r, c) - \text{erosion}_{a2}(r, c))|, \\ & |(f(r, c) - \text{erosion}_{a3}(r, c)) - (f(r, c) \\ & - \text{erosion}_{a4}(r, c))|\}. \end{aligned} \quad (20)$$

We apply this operator on the same edge and noise patterns that we used in the previous section. The results are

$$\begin{matrix} 0 & 0 & 0 & 0 & 0 \\ 0 & 0 & 0 & 0 & 0 \\ E & E & E & E & E \\ 0 & 0 & 0 & 0 & 0 \\ 0 & 0 & 0 & 0 & 0 \end{matrix} \qquad \begin{matrix} 0 & 0 & E & 0 & 0 \\ 0 & 0 & E & 0 & 0 \\ 0 & 0 & E & 0 & 0 \\ 0 & 0 & E & 0 & 0 \\ 0 & 0 & E & 0 & 0 \end{matrix}$$

$E_{0°}$ $E_{90°}$

$$\begin{matrix} 0 & 0 & 0 & 0 & E \\ 0 & 0 & 0 & E & 0 \\ 0 & 0 & E & 0 & 0 \\ 0 & E & 0 & 0 & 0 \\ E & 0 & 0 & 0 & 0 \end{matrix} \qquad \begin{matrix} E & 0 & 0 & 0 & 0 \\ 0 & E & 0 & 0 & 0 \\ 0 & 0 & E & 0 & 0 \\ 0 & 0 & 0 & E & 0 \\ 0 & 0 & 0 & 0 & E \end{matrix}$$

$E_{45°}$ $E_{135°}$

$$\begin{matrix} 0 & 0 & E/2 & E/2 & 0 \\ 0 & 0 & E/2 & E/2 & 0 \\ 0 & 0 & E/2 & E/2 & 0 \\ 0 & 0 & E/2 & E/2 & 0 \\ 0 & 0 & E/2 & E/2 & 0 \end{matrix} \qquad \begin{matrix} 0 & 0 & 0 & 0 & 0 \\ 0 & 0 & 0 & 0 & 0 \\ 0 & 0 & 0 & 0 & 0 \\ 0 & 0 & 0 & 0 & 0 \\ 0 & 0 & 0 & 0 & 0 \end{matrix}$$

$E_{r0°}$ noise 1

$$\begin{matrix} 0 & 0 & 0 & 0 & 0 \\ 0 & 0 & 0 & 0 & 0 \\ 0 & 0 & 0 & 0 & 0 \\ 0 & 0 & 0 & 0 & 0 \\ 0 & 0 & 0 & 0 & 0 \end{matrix}$$

noise 2

Like $G_e(r, c)$, $G_e'(r, c)$ assigns edge strength E to all the edge points which are on the high value side of the ideal step edge and detects two edge lines of half-edge contrast from ideal ramp edge patterns. However, unlike the simple erosion residue operator, it will not pick up the noise pixel. Hence this is an improved version of the $G_e(r, c)$ operator.

3) Putting G_e' and G_d' Together: It is natural that an improved version of the morphologic edge operator which has no position bias and is noise insensitive will be a combination of the improved dilation residue and erosion residue operators. Consider the sum of these two:

$$E'(r, c) = G_e'(r, c) + G_d'(r, c). \tag{21}$$

The results of this operator applied to the same test patterns are

$$\begin{matrix} 0&0&0&0&0 \\ 0&0&0&0&0 \\ E&E&E&E&E \\ E&E&E&E&E \\ 0&0&0&0&0 \end{matrix} \qquad E_{0°}$$

$$\begin{matrix} 0&0&E&E&0 \\ 0&0&E&E&0 \\ 0&0&E&E&0 \\ 0&0&E&E&0 \\ 0&0&E&E&0 \end{matrix} \qquad E_{90°}$$

$$\begin{matrix} 0&0&0&0&E \\ 0&0&0&E&E \\ 0&0&E&E&0 \\ 0&E&E&0&0 \\ E&E&0&0&0 \end{matrix} \qquad E_{45°}$$

$$\begin{matrix} E&0&0&0&0 \\ E&E&0&0&0 \\ 0&E&E&0&0 \\ 0&0&E&E&0 \\ 0&0&0&E&E \end{matrix} \qquad E_{135°}$$

$$\begin{matrix} 0&E/2&E&E/2&0 \\ 0&E/2&E&E/2&0 \\ 0&E/2&E&E/2&0 \\ 0&E/2&E&E/2&0 \\ 0&E/2&E&E/2&0 \end{matrix} \qquad E_{r0°}$$

$$\begin{matrix} 0&0&0&0&0 \\ 0&0&0&0&0 \\ 0&0&0&0&0 \\ 0&0&0&0&0 \\ 0&0&0&0&0 \end{matrix} \qquad \text{noise 1}$$

$$\begin{matrix} 0&0&0&0&0 \\ 0&0&0&0&0 \\ 0&0&0&0&0 \\ 0&0&0&0&0 \\ 0&0&0&0&0 \end{matrix} \qquad \text{noise 2}$$

The operator has perfect performance on ideal step edges and single noise patterns. Thresholding with a threshold value greater than $E/2$ perfectly detects ideal ramp edges. The shortcoming of this operator is that it works only on a 3×3 local neighborhood. Thus its capability for reducing the effects of noise is limited.

B. Blur and Minimum Operator

This morphological edge operator is defined by

$$I_{\text{edge-strength}} = \min \{I_1 - \text{erosion } (I_1), \text{ dilation } (I_1) - I_1\} \tag{22}$$

where I_1 = blur $\{I_{\text{input}}\}$ and blur $\{I_{\text{input}}\}$ is the input image with a blurring operation. We use the same neighborhood size for both the kernel of the blur and the structuring element of the dilation and erosion.

Consider the following one-dimensional step edge sequence as a motivation for this definition. In this sequence, the blur uses a neighborhood of width three, and the erosion and dilation use a flat structuring element having domain $\{-1, 0, 1\}$.

original	0	0	0	0	E	E	E
blur	0	0	0	$\frac{E}{3}$	$\frac{2E}{3}$	E	E
erosion of blur	0	0	0	0	$\frac{E}{3}$	$\frac{2E}{3}$	E
dilation of blur	0	0	$\frac{E}{3}$	$\frac{2E}{3}$	E	E	E.
blur-erosion	0	0	0	$\frac{E}{3}$	$\frac{E}{3}$	$\frac{E}{3}$	0
dilation-blur	0	0	$\frac{E}{3}$	$\frac{E}{3}$	$\frac{E}{3}$	0	0
edge strength	0	0	0	$\frac{E}{3}$	$\frac{E}{3}$	0	0

The advantage of this operator, as illustrated below, is that it will not detect a single noise point:

original	0	0	0	N	0	0	0
blur	0	0	$\frac{N}{3}$	$\frac{N}{3}$	$\frac{N}{3}$	0	0
erosion of blur	0	0	0	$\frac{N}{3}$	$\frac{N}{3}$	0	0
dilation of blur	0	$\frac{N}{3}$	$\frac{N}{3}$	$\frac{N}{3}$	$\frac{N}{3}$	0	0.
blur-erosion	0	0	$\frac{N}{3}$	0	0	0	0
dilation-blur	0	$\frac{N}{3}$	0	0	0	0	0
edge strength	0	0	0	0	0	0	0

Now let us examine the performance of this operator on ideal ramp edge sequences. Let a_i be a one-dimensional sequence which has $a_i = 0$ for all $i \leq 0$ and $a_i = E$ for all $i > 5$. Let $a_i \geq a_j$, for all $i > j$, $i, j \in \{1, \cdots, 5\}$. Let the sequence e_i be the result of applying a blur-minimum operation of three point support to the sequence a_i. Then

$$e_i = 0 \text{ for all } i < 0$$

$$e_0 = \frac{a_1}{3}\ ;\ e_1 = \frac{a_2}{3}$$

$$e_2 = \frac{\min (a_3,\ a_4 - a_1)}{3}$$

$$e_3 = \frac{\min (a_4 - a_1,\ a_5 - a_2)}{3} \tag{23}$$

$$e_4 = \frac{\min (a_5 - a_2,\ E - a_3)}{3}$$

$$e_5=\frac{E-a_4}{3}\ ;\ e_6=\frac{E-a_5}{3}$$

$$e_i=0 \text{ for all } i>6.$$

Thus, for an ideal ramp edge of three pixels ($a_1 = a_2 = 0$, $a_3 = E/2$, $a_4 = a_5 = E$), the edge strength will be

e_0	e_1	e_2	e_3	e_4	e_5	e_6
0	0	$\frac{E}{6}$	$\frac{E}{3}$	$\frac{E}{6}$	0	0

For an ideal ramp edge of four pixels ($a_1 = a_2 = 0$, $a_3 = E/3$, $a_4 = 2E/3$, $a_5 = E$), the edge strength will be

e_0	e_1	e_2	e_3	e_4	e_5	e_6
0	0	$\frac{E}{9}$	$\frac{2E}{9}$	$\frac{2E}{9}$	$\frac{E}{9}$	0

For an ideal ramp edge of five pixels ($a_1 = 0$, $a_2 = E/4$, $a_3 = E/2$, $a_4 = 3E/4$, $a_5 = E$), the edge strength will be

e_0	e_1	e_2	e_3	e_4	e_5	e_6
0	$\frac{E}{12}$	$\frac{E}{6}$	$\frac{E}{4}$	$\frac{E}{6}$	$\frac{E}{12}$	0

For an ideal ramp edge of six pixels ($a_1 = E/5$, $a_2 = 2E/5$, $a_3 = 3E/5$, $a_4 = 4E/5$, $a_5 = E$), the edge strength will be

e_0	e_1	e_2	e_3	e_4	e_5	e_6
$\frac{E}{15}$	$\frac{2E}{15}$	$\frac{E}{5}$	$\frac{E}{5}$	$\frac{2E}{15}$	$\frac{E}{15}$	0

For an ideal ramp edge of seven pixels ($a_1 = E/6$, $a_2 = E/3$, $a_3 = E/2$, $a_4 = 2E/3$, $a_5 = 5E/6$), the edge strength will be

e_0	e_1	e_2	e_3	e_4	e_5	e_6
$\frac{E}{18}$	$\frac{E}{9}$	$\frac{E}{6}$	$\frac{E}{6}$	$\frac{E}{6}$	$\frac{E}{9}$	$\frac{E}{18}$

The blur-minimum morphologic edge operator is noise insensitive. For the ideal step edge, it produces a result which has nonzero edge strength on both the edge pixels. This is consistent with the fact that an ideal step edge line should be two pixels in width. However, due to the effect of blurring, the edge strength assigned to the edge pixels is one third the edge contrast. For ideal ramp edges of larger spatial extent, it will assign a significant nonzero edge strength to more than one pixel. However, the true edge pixel is usually given a higher edge strength than its neighbors. Thus, by thresholding the edge strength image with a suitable threshold value, we can extract the ideal ramp edges. It is also noted that as the spatial extent of the ideal ramp edge increases, the edge contrast of the detected edge point decreases. For the case of a seven pixel ramp edge, the detected edge strength of the edge point is the same as the edge strength of its immediate adjacent pixels.

The reason why we need a small amount of blurring is that this operator only assigns a pixel to be an edge pixel if it has a value in the middle between two gray-scale extremes of the neighborhood centered at the given pixel. Thus there must be significant differences in gray-scale value between the pixel and both its nearby gray-scale maximum and nearby gray-scale minimum pixels. The edge pixels are the two pixels on either side of the jump. For the ideal step edge, these pixels are a local maximum and minimum. Hence this operator cannot detect the ideal step edges unless we blur the ideal step edge before applying it.

To have a better understanding of this edge operator, we give a derivation which explains this operator as an easily understandable local neighborhood nonlinear operator. Let K be the neighborhood size of the kernel of the blur and the domain of the structuring element. Without loss of generality, we assume that K is an odd number. Let $L = (K-1)/2$, and b_i = blur (a_i), $e_i = b_i -$ erosion (a_i), d_i = dilation $(a_i) - b_i$. Then

$$b_i=\frac{\sum_{p=i-L}^{i+L} a_p}{K}$$

$$\begin{aligned} e_i &= \max_{q\in\{0,\cdots,K-1\}} \{b_i - b_{i+L-q}\} \\ &= \frac{1}{K} \max_{q\in\{1,\cdots,L\}} \left\{\left(-\sum_{p=1}^{q} a_{i+L+p}+\sum_{p=1}^{q} a_{i-L-1+p}\right), \right. \\ &\quad \left.\left(\sum_{p=1}^{q} a_{i+L+1-p}-\sum_{p=1}^{q} a_{i-L-p}\right), 0\right\}, \end{aligned}$$

and

$$\begin{aligned} d_i &= \max_{q\in\{0,\cdots,K-1\}} \{b_{i+L-q} - b_i\} \\ &= \frac{1}{K} \max_{q\in\{1,\cdots,L\}} \left\{\left(-\sum_{p=1}^{q} a_{i-L-1+p}+\sum_{p=1}^{q} a_{i+L+p}\right), \right. \\ &\quad \left.\left(\sum_{p=1}^{q} a_{i-L-p}-\sum_{p=1}^{q} a_{i+L+1-p}\right), 0\right\}. \end{aligned} \tag{24}$$

For example, with $K = 3$, we define four one-dimensional five-point masks:

$$A_1=\frac{1}{3} * [-1 \quad 0 \quad 0 \quad 1 \quad 0]$$

$$A_2=\frac{1}{3} * [\ 0 \quad 1 \quad 0 \quad 0 \quad -1]$$

$$A_3=\frac{1}{3} * [\ 1 \quad 0 \quad 0 \quad -1 \quad 0]$$

$$A_4=\frac{1}{3} * [\ 0 \quad -1 \quad 0 \quad 0 \quad 1].$$

Then the edge detector becomes

$$\min \{\max \{A_1 * f, A_2 * f\}, \max \{A_3 * f, A_4 * f\}\} \tag{25}$$

where f is the input data and $*$ is the convolution operation.

In the case that $K = 5$, we define eight one-dimensional nine-point masks:

$$A_1 = \frac{1}{5} * [\ 0\ \ -1\ \ 0\ \ 0\ \ 0\ \ 0\ \ 1\ \ 0\ \ 0]$$

$$A_2 = \frac{1}{5} * [-1\ \ -1\ \ 0\ \ 0\ \ 0\ \ 1\ \ 1\ \ 0\ \ 0]$$

$$A_3 = \frac{1}{5} * [\ 0\ \ 0\ \ 1\ \ 0\ \ 0\ \ 0\ \ 0\ \ -1\ \ 0]$$

$$A_4 = \frac{1}{5} * [\ 0\ \ 0\ \ 1\ \ 1\ \ 0\ \ 0\ \ 0\ \ -1\ \ -1]$$

$$A_5 = \frac{1}{5} * [\ 0\ \ 1\ \ 0\ \ 0\ \ 0\ \ 0\ \ -1\ \ 0\ \ 0]$$

$$A_6 = \frac{1}{5} * [\ 1\ \ 1\ \ 0\ \ 0\ \ 0\ \ -1\ \ -1\ \ 0\ \ 0]$$

$$A_7 = \frac{1}{5} * [\ 0\ \ 0\ \ -1\ \ 0\ \ 0\ \ 0\ \ 0\ \ 1\ \ 0]$$

$$A_8 = \frac{1}{5} * [\ 0\ \ 0\ \ -1\ \ -1\ \ 0\ \ 0\ \ 0\ \ 1\ \ 1].$$

Then, the edge detector becomes

$$\min \{\max \{A_1 * f, A_2 * f, A_3 * f, A_4 * f\}, \max \{A_5 * f, A_6 * f, A_7 * f, A_8 * f\}, 0\}. \quad (26)$$

This operator finds the difference between each side of a given point. Instead of considering only the difference of the average pixel intensity on both sides of a pixel, it considers differences of varieties of local structures and combines the result of each difference by maximizations and a minimization operation. Thus by increasing the neighborhood size of the blur operator and the neighborhood size of the morphologic operation, this operator can reduce the effects of noise and yet not blur the edges too much.

V. Experimental Results

To understand the performance of the morphologic edge operators, we examine their behavior on two simulated images. We also compare the results of the morphologic edge operators with the cubic facet second derivative edge operator (Haralick [10]) and ten enhancement/thresholding edge detectors (Abdou and Pratt [1]).

The first simulated image is an image which has ten distorted square boxes. To simulate edges of different directions, the left side of the square boxes are tilted such that their corresponding edge lines have directions ranging from 0° to 45°. The edge contrast of these edges is 50, and the box size is 50 × 50 pixels. To this image, we add independent Gaussian noise having mean zero and standard deviation 15. The original and noisy images are shown in Fig. 1.

To compare the performance of different edge operators,

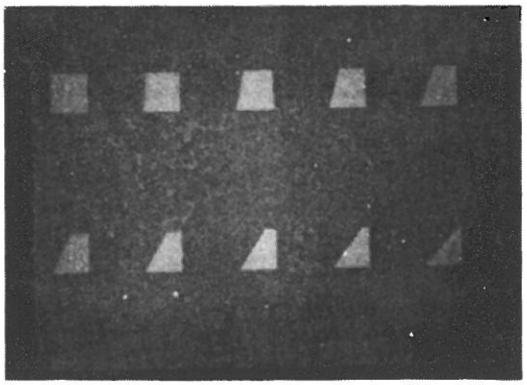

Fig. 1. Image containing ten boxes of different edge directions and noisy images with $\sigma_n = 15.0$. Edge contrast is 50.

TABLE I
$P(E'|E^*)$ AND $P(E^*|E')$ VALUES OF MORPHOLOGIC EDGE OPERATORS AND CUBIC FACET EDGE OPERATORS

Operator/Probability	$P(E'\|E^*)$	$P(E^*\|E')$
Maximum	0.2911	0.2953
Improved sum	0.4565	0.4380
Blur-minimum (5 × 5)	0.7870	0.7870
Blur-minimum (9 × 9)	0.9587	0.9350
Blur-minimum (13 × 13)	0.9061	0.9369
Facet edge (5 × 5)	0.8387	0.8256
Facet edge (9 × 9)	0.9355	0.9063

we use the conditional probability of the label "edge" given the true edge $P(E'|E^*)$ and the conditional probability of a true edge given the label edge, $P(E^*|E')$. The adjustable parameters of each edge operator are chosen to equalize these two conditional probabilities. The quality of the edge operator is determined by the value of $P(E'|E^*) = P(E^*|E')$. Although this performance measure is not in general applicable on all kinds of images, it is well-suited for this simulated image.

We apply the maximum version (12), the improved summation version (21), and the blur-minimum version (22) of the morphologic edge detectors and the cubic facet second derivative zero-crossing edge operator on the noisy square boxes and compare the performance in terms of $P(E'|E^*)$ and $P(E^*|E')$. The neighborhood supports for the blur-minimum operators used are 3 × 3, 5 × 5, and 7 × 7, respectively. The effective neighborhood sizes are 5 × 5, 9 × 9, and 13 × 13, because a blur is applied before the morphologic operations are actually applied to an image. From here on, we will use the effective neighborhood size to name each operation. The neighborhood sizes for the cubic facet edge detector are 5 × 5 and 9 × 9, respectively.

Table I lists the test results of these edge operators. To ignore image border effects, the performance probabilities are measured in a window of size 490 × 390. The performance probability of the maximum version of the morphologic edge operator is only 29 percent. The improved summation version of the morphologic edge operator increases the probability to 45 percent. The performance of the blur-minimum version of the morphologic edge operator is superior. The probability is increased to 78 percent, 94 percent, and 92 percent for 5 × 5,

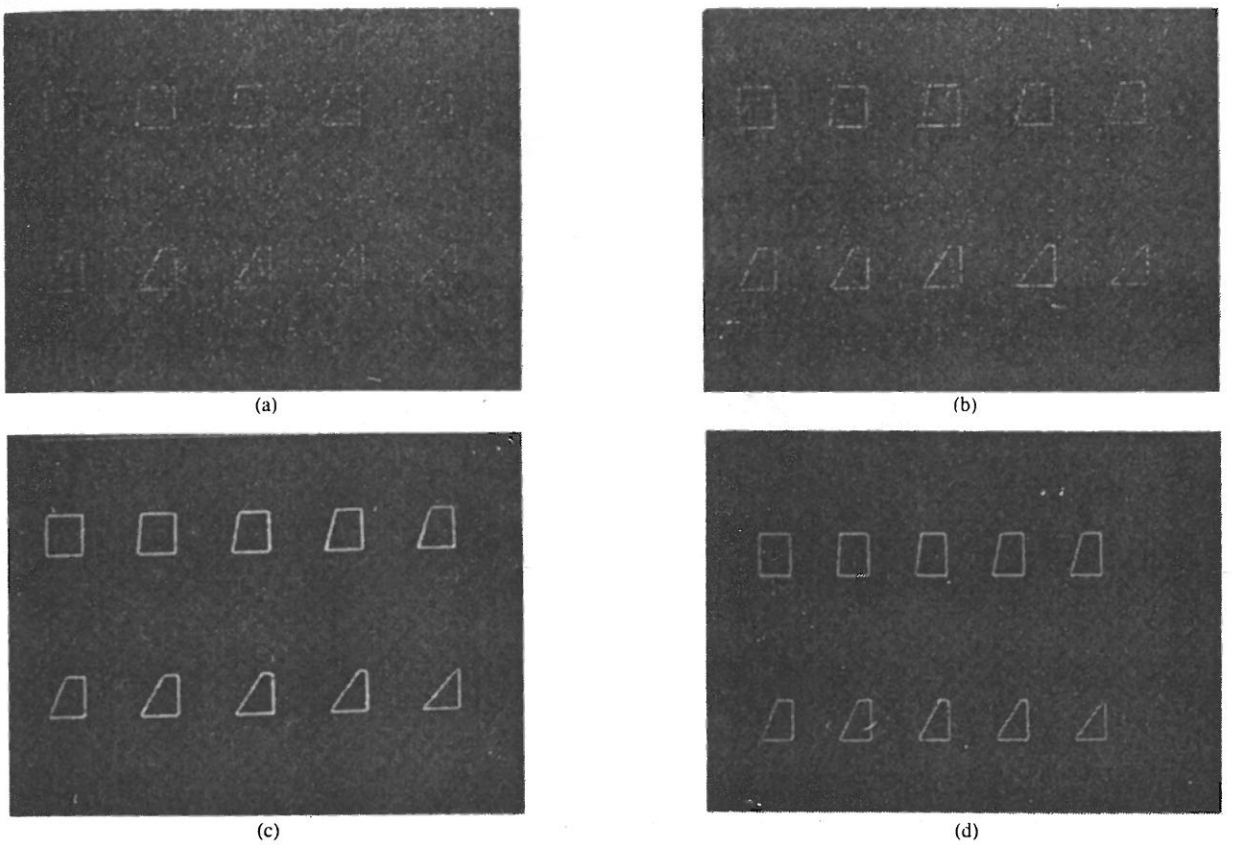

Fig. 2. Edge results of different edge operators applied on square box image. (a) Maximum version morphologic edge operator. (b) Improved summation version morphologic edge operator. (c) Blur-minimum version (9 × 9) morphological edge operator. (d) Cubic facet second derivative zero-crossing edge operator with 9 × 9 neighborhood.

9 × 9, and 13 × 13 neighborhood support, respectively. This is because the blur-minimum operators have a larger number of pixels involved in the edge detection than just a 3 × 3 neighborhood. Similarly, the cubic facet second derivative zero-crossing edge operator also makes use of larger than 3 × 3 neighborhood support, and it performs well. Its performance probabilities are about 82 percent and 92 percent for the 5 × 5 and 9 × 9 neighborhoods, respectively.

Fig. 2(a)–(d) show the results of the maximum version, the improved summation version, and the blur-minimum (9 × 9) version of the morphologic edge operators and the cubic facet edge operator (9 × 9).

A visual evaluation also leaves the impression that the blur-minimum edge detector and the cubic facet second derivative zero-crossing edge operator produce much better edge continuity and have less sensitivity to noise than the other edge detectors.

The second simulated image is a checkerboard of size 100 × 100 pixels with a check size of 20 × 20 pixels. The dark checks have gray-scale intensity 50, and the light checks have gray-scale intensity 100. To this perfect checkerboard, we add independent Gaussian noise having mean zero and standard deviation 7.5, 15.0, and 30.0, respectively. Thus the signal to noise ratios (SNR = edge contrast/noise deviation) of these images are 6.67, 3.33, and 1.67, respectively. The perfect and noisy checkerboards are shown in Fig. 3.

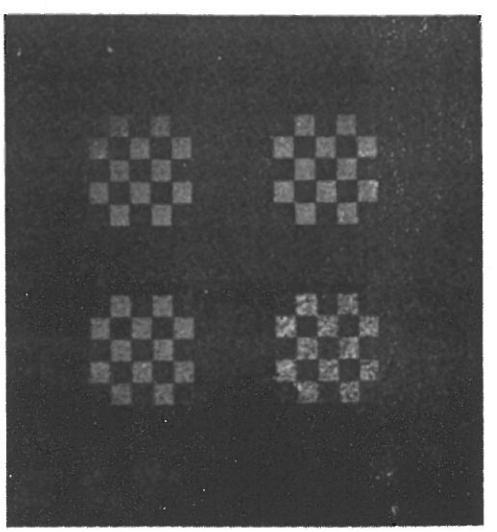

Fig. 3. Perfect checkerboard image and its noisy images. From left to right, top to bottom: perfect image, SNR = 6.67, SNR = 3.33, and SNR = 1.67, respectively. Image size is 100 × 100 pixels. Check size in 20 × 20 pixels. Edge contrast is 50, and added noise is zero mean Gaussian noise.

To compare the performance of the morphologic-based edge operators with the nonmorphologic based edge operator, we apply the cubic facet based second directional derivative zero-crossing edge operator, ten enhancement/thresholding edge detectors, and the maximum, improved summation, and blur-minimum versions of the morphologic edge operator on the noisy checkerboard images and compare the performance

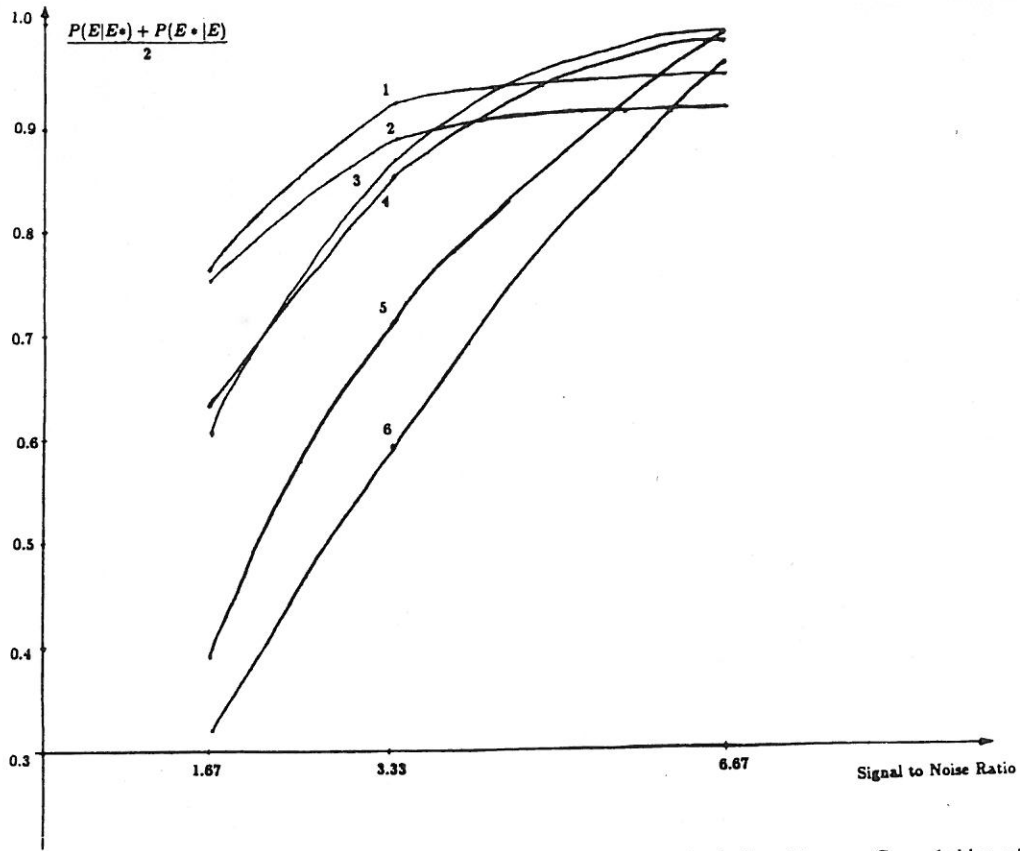

Fig. 4. Performance probabilities of facet and morphologic edge operators on noisy checkerboard images. Curve 1: blur-minimum morphologic edge operator of 9 × 9 equivalent support. Curve 2: second derivative zero-crossing edge operator of 9 × 9 support. Curve 3: blur-minimum morphologic edge operator of 5 × 5 equivalent support. Curve 4: second derivative zero-crossing edge operator of 5 × 5 support. Curve 5: improved summation morphologic edge operator. Curve 6: maximum morphologic edge operator.

in terms of $P(E'|E^*)$ and $P(E^*|E')$. The structuring element for the maximum and improved summation morphologic edge operators is a rod of radius 1 which has four connected pixels as its neighborhood support. The neighborhood supports for the blur-minimum operator are 5 × 5 and 9 × 9, respectively. The window sizes of the cubic polynomial fitting for the second derivative zero-crossing operator are 5 × 5 and 9 × 9, respectively. There are two types of spatial edge enhancement operators: the differential and the template matching operators. The differential operators we used are Roberts, Prewitt, and Sobel operators. The template matching operators we used are compass gradient, Kirsch, and three- and five-level template mask operators (Abdou and Pratt [1]).

Fig. 4 plots the probability results of the morphologic and the cubic facet zero-crossing edge operators. The results show that the second derivative zero-crossing edge operator and the blur-minimum morphologic edge operator have much better performance than the other morphologic operators. When the SNR is large, the blur-minimum edge operator of 5 × 5 neighborhood size and the cubic facet zero-crossing edge operator perform best. As the SNR becomes small, the blur-minimum edge operator having a 9 × 9 neighborhood size and the cubic facet zero-crossing edge operator perform best. The improved summation morphologic edge operator has good performance when the SNR is large. As the SNR decreases its performance probability decreases dramatically and soon becomes much worse than the zero-crossing and blur-minimum operators. The maximum version of the morphologic edge operator has the worst performance among all these operators.

Fig. 5 plots the probability results of the differential operators. Two different methods of gradient computation are used for each operator: root mean squared and absolute sum. The results show that the Roberts operators perform worse than the other operators. The Prewitt operator performs better than the Sobel operator, and the rms gradient is better than the absolute summation. When compared with the morphologic edge detector, all the differential operators perform much worse than the blur-minimum morphologic operators, when a significant amount of noise is injected into the testing image.

Fig. 6 plots the probability results of the template operators. The results show that the compass operators perform worse than the other operators. The Kirsch operator performs best among the template operators. The three-level operator exceeds the five-level operator in performance when the SNR is large. When the SNR is small, both operators have similar performance. All the template operators perform much worse than the blur-minimum morphologic operators as a significant amount of noise is added to the test images.

The performance of the edge operators can be explained in terms of the neighborhood size we used for each operator. Both the blur-minimum edge operator with 9 × 9 support and the 9 × 9 cubic facet second derivative zero-crossing edge operator involve 81 pixels in the edge detection process to

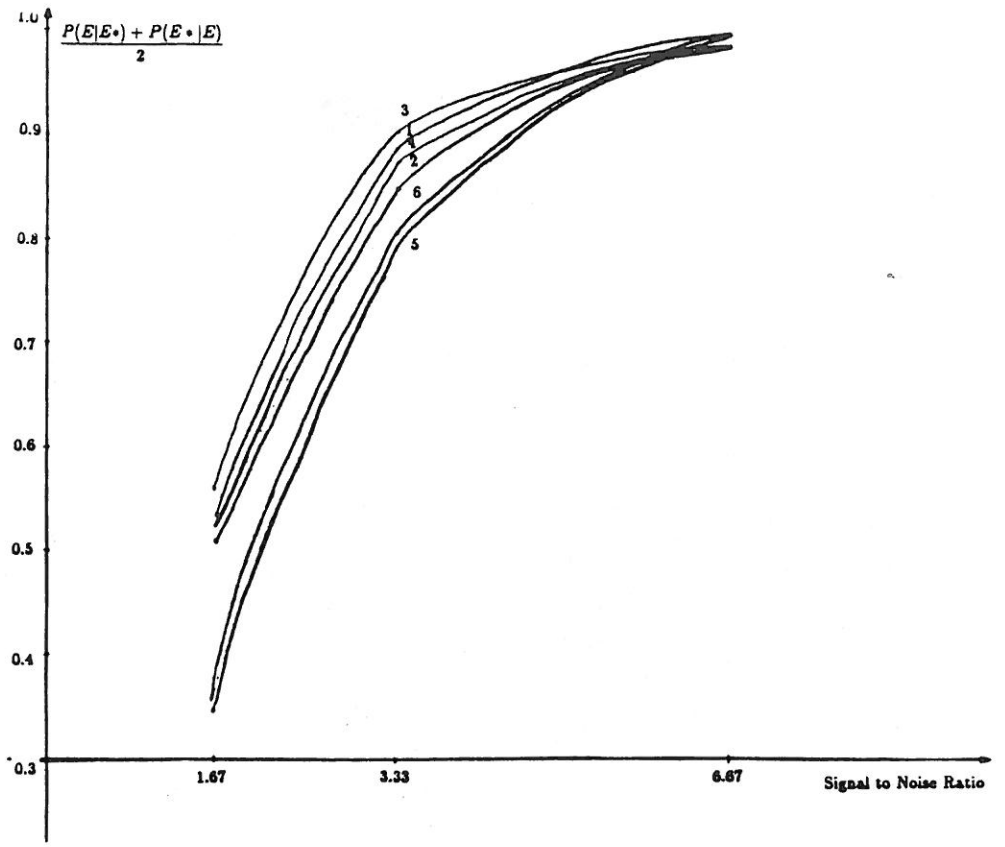

Fig. 5. Performance probabilities of differential edge operators on noisy checkerboard images. Curve 1: Sobel rms gradient. Curve 2: Sobel absolute summation. Curve 3: Prewitt rms gradient. Curve 4: Prewitt absolute summation. Curve 5: Roberts rms gradient. Curve 6: Roberts absolute summation.

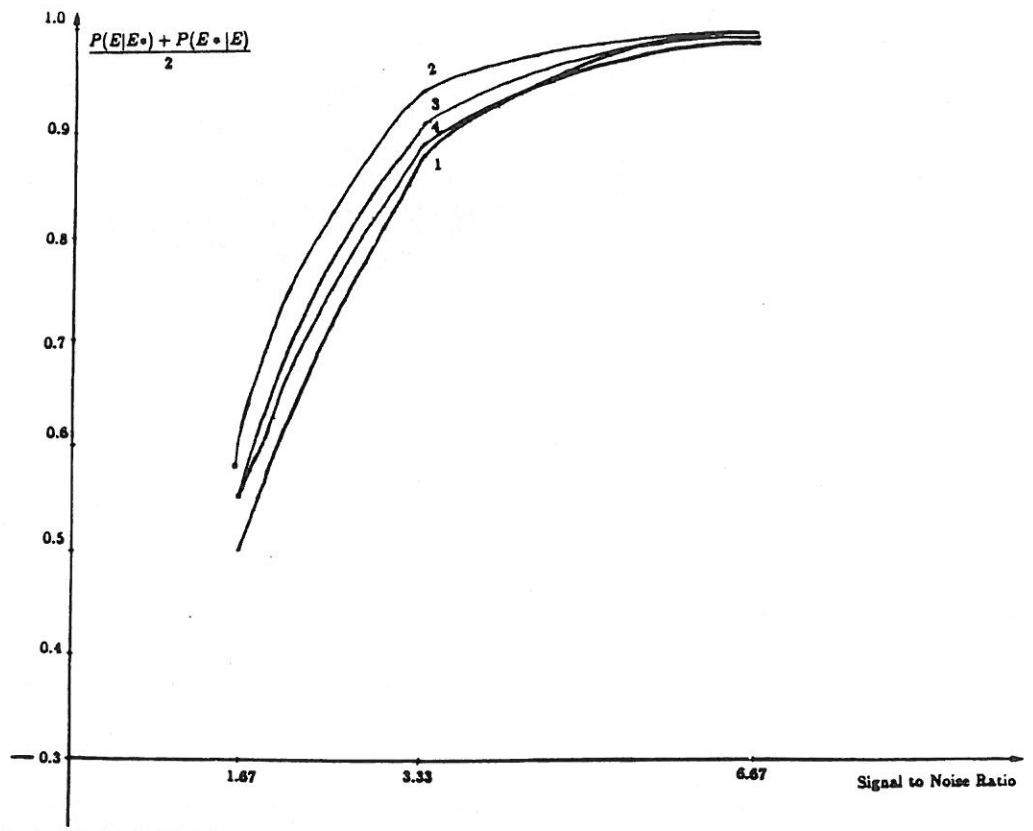

Fig. 6. Performance probabilities of template edge operators on noisy checkerboard images. Curve 1: compass template operator. Curve 2: Kirsch template operator. Curve 3: three-level template operator. Curve 4: five-level template operator.

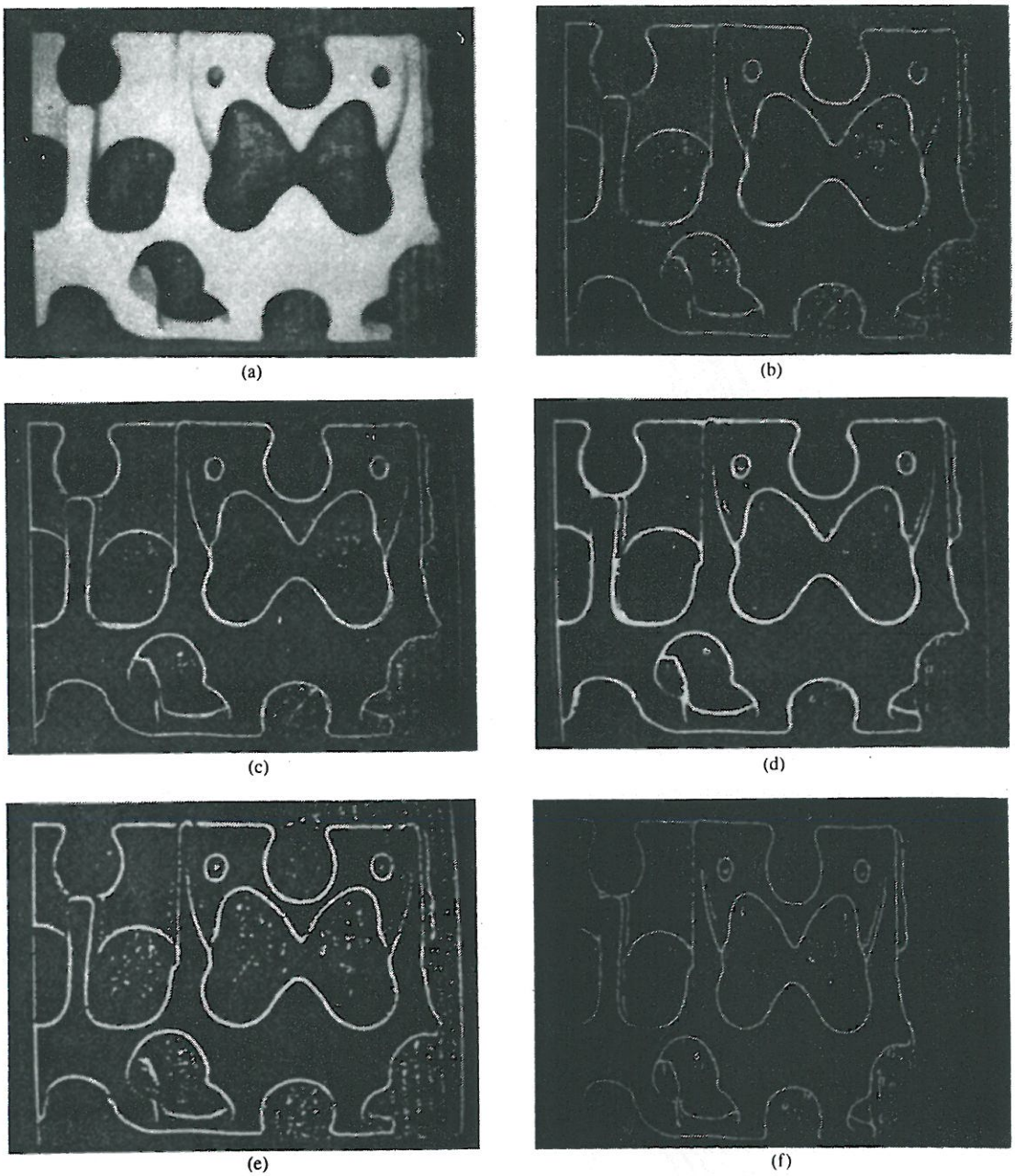

Fig. 7. (a) Sand casting mold image and its edge image. (b) Edge image of maximum version morphologic edge operator. (c) Edge image of improved summation morphologic edge operator. (d) Edge image of 9 × 9 blur-minimum morphologic edge operator. (e) Edge image of difference of Gaussian edge operator. (f) Edge image of 9 × 9 cubic facet edge operator.

assign the edge state of a single pixel. Due to the large neighborhood size, they have the best performance as the noise increases. The 5 × 5 blur-minimum morphologic edge operator and the 5 × 5 cubic facet second derivative zero-crossing edge operator involve 25 pixels in the edge detection process. They have good performance when the noise is small. As the noise increases, their performance is worse than those with a larger neighborhood size. However, their performance is better than the performance of the enhancement/thresholding edge detectors and the improved summation morphologic edge operator which involves only nine pixels and the maximum version morphologic edge operator which involves only five pixels in the edge detection process.

Note that when the noise is small, an edge operator with small neighborhood support such as the improved summation operator or the Roberts edge operator is good enough. However, as the SNR becomes small, we have to use edge operators of larger neighborhood support. Since the performance of the blur-minimum morphologic edge operator is comparable to the zero-crossing edge operator, it will be very useful in those applications which need large neighborhood support, but cannot afford the higher computational cost of the facet edge operator.

Finally, we illustrate an example of the morphologic edge detectors applied on a real image. The image is a mold for sand casting shown in Fig. 7(a). We apply the maximum, the

improved summation, and the blur-minimum morphologic edge detectors with 9 × 9 support, a difference of Gaussian operator with circular support of diameter 40 and 24 pixels, and the cubic facet second derivative zero-crossing operator with window size 9 × 9 to this image. The resulting edge images are shown in Fig. 7(b)–(f). A visual evaluation leaves the impression that the cubic facet edge operator and the blur-minimum morphologic edge detector have the best performance. The difference of Gaussian operator produces thick edge lines and the edge connectivity is not as good as the blur-minimum edge operator. The improved summation edge operator is better than the maximum version edge operator. Both of them are noisier than the cubic facet and the blur-minimum edge operator.

VI. Conclusion

We have introduced some edge operators based on gray-scale morphologic operations. These operators can be efficiently implemented in many machine vision systems which have special hardware support for morphologic operations. The simplest edge detectors are dilation residue and erosion residue operators. Different combinations of these two simple operators have been introduced and justified. Finally, some operators which are insensitive to noise have been introduced.

Experimental results show the validity of the blur-minimum morphologic edge operator. Upon comparing the performance of the morphologic edge detectors with the enhancement/thresholding edge detectors and the cubic facet second derivative zero-crossing edge operator, we found that when the noise is small, all the edge operators have similar performance. However, as the noise increases, the second derivative zero-crossing edge operator and the blur-minimum morphologic edge operator perform best. The blur-minimum morphologic edge operator has performance comparable with the second derivative zero-crossing edge operator and it is less computationally expensive. Thus it provides an efficient way to extract good edges from noisy images.

References

[1] I. E. Abdou and W. K. Pratt, "Quantitative design and evaluation of enhancement/thresholding edge detectors," *Proc. IEEE*, vol. 67, May 1979.

[2] M. J. Brooks, "Rationalizing edge detectors," *Comput. Graphics Image Processing*, vol. 8, pp. 277–285, 1978.

[3] G. P. Dineen, "Programming pattern recognition," in *Proc. Western Joint Computer Conf.*, 1955, pp. 94–100.

[4] R. O. Duda and P. E. Hart, *Pattern Classification and Scene Analysis*. New York: Wiley, 1973.

[5] J. Foglein, "On edge gradient approximations," *Pattern Recognition Lett.*, pp. 429–434, 1983.

[6] M. Golay, "Hexagonal parallel pattern transformations," *IEEE Trans. Comput.*, vol. C-18, pp. 733–740, 1969.

[7] R. Haralick, "Edge and region analysis for digital image data," *Comput. Graphics Image Processing*, vol. 12, pp. 60–73, 1980.

[8] ——, "The digital edge," in *Proc. IEEE 1981 Conf. Pattern Recognition Image Processing*. New York: IEEE Computer Society, 1981, pp. 285–294.

[9] ——, "Zero-crossing of second directional derivative edge operator," presented at the Soc. Photogrammetric Instrumentation Engineers Symp. Robot Vision, Washington, DC, May 1982.

[10] ——, "Digital step edges from zero crossing of second directional derivatives," *IEEE Trans. Pattern Anal. Machine Intell.*, vol. PAMI-6, pp. 58–68, Jan. 1984.

[11] R. Haralick and J. Lee, "Neighborhood context dependent edge detection," *IEEE Trans. Pattern Anal. Machine Intell.*, to be published.

[12] M. Hueckel, "An operator which locates edges in digitized pictures," *J. Assoc. Comput. Mach.*, vol. 18, pp. 113–25, 1971.

[13] ——, "A local visual operator which recognizes edges and lines," *J. Assoc. Comput. Mach.*, vol. 20, pp. 634–647, 1973.

[14] R. A. Hummel, "Feature detectioning basis functions," *Comput. Graphics Image Processing*, vol. 9, pp. 40–55, 1979.

[15] R. A. Kirsch, "Experiments in processing lifemotion with a digital computer," in *Proc. Eastern Joint Computer Conf.*, 1957, pp. 221–229.

[16] R. Kirsch, "Computer determination of the constituent structure of biological images," *Comput. Biomed., Res.*, 4, pp. 315–328, 1971.

[17] R. M. Landsman, L. B. Scott, and M. J. E. Golay, "Apparatus for counting bi-nucleate lymplocytes in blood," US Patent 3 214 574, filed Oct. 8, 1959, issued Oct. 26, 1965.

[18] *Genesis 2000 BLIX Language Manual*, Version 1.0, Machine Vision International Corp., 1984.

[19] D. Marr and E. Hildreth, "Theory of edge detection," *Proc. Roy. Soc. London*, B, vol. 207, pp. 187–217, 1980.

[20] A. Martelli, "An application of heuristic search methods to edge and contour detection," *Commun. Ass. Comput. Mach.*, vol. 19, pp. 73–83, Feb. 1976.

[21] G. Matheron, "Random sets and integral," in *Geometry*. New York: Wiley, 1975.

[22] J. W. Modestino and R. W. Fries, "Edge detection in noisy images using recursive digital filtering," *Comput. Graphics Image Processing*, vol. 6, pp. 409–433, 1977.

[23] U. Montanari, "On the optimal detection of curves in noisy pictures," *Commun. Ass. Comput. Mach.*, vol. 14, pp. 335–345, May 5, 1971.

[24] G. A. Moore, "Applications of computers to quantitative analysis of microstructure," U.S.W.B.S. Rep. 9428, 1966.

[25] ——, "Automatic sensing and computer process for the quantitative analysis of micrographs and equivalued subjects," in *Picturial Pattern Recognition*. Thompson Book Co., 1968, pp. 275–326.

[26] D. Morgenthaler, "A new hybrid edge detector," *Comput. Graphics Image Processing*, vol. 16, pp. 166–176, 1981.

[27] D. Morgenthaler and A. Rosenfeld, "Multidimensional edge section by hypersurface fitting," *IEEE Trans. Pattern Anal. Machine Intell.*, vol. PAMI-3, pp. 482–486, July 1981.

[28] K. T. Preston, "The cellscon system—A lencocyte pattern analyzer," in *Proc. Western Joint Comput. Conf.*, 1961, pp. 175–178.

[29] ——, "Feature extraction by Golay hexagonal pattern transforms," *IEEE Trans. Comput.*, vol. C-20, pp. 1007–1014, 1971.

[30] ——, "Multidimensional logical transforms," *IEEE Trans. Pattern Anal. Machine Intell.*, vol. PAMI-5, pp. 539–554, Sept. 1983.

[31] J. Prewitt, "Object enhancement and extraction," in *Picture Processing and Psychopictorics*, B. Lipkin and A. Rosenfeld, Eds. New York: Academic, 1970, pp. 75–149.

[32] G. S. Robinson, "Edge detection by compass gradient masks," *Comput. Graphics Image Processing*, vol. 6, pp. 492–501, 1977.

[33] A. Rosenfeld and A. Kak, *Digital Picture Processing*, vol. 2. New York: Academic, 1982.

[34] J. Serra, *Image Analysis and Mathematical Morphology*. London: Academic, 1982.

[35] K. S. Shanmugam, F. M. Dickey, and J. A. Green, "An optimal frequency domain filter for edge detection in digital pictures," *IEEE Trans. Pattern Anal. Machine Intell.*, vol. PAMI-1, pp. 37–49, 1979.

[36] S. R. Sternberg, "Cellular computers and biomedical image processing," in *Lecture Notes in Medical Informations, vol. 17: Biomedical Images and Computers, Proceedings 1980*, J. Sklansky and J. C. Bisconte, Eds. Berlin: Springer-Verlag, 1980, pp. 294–319.

[37] ——, "Languages and architectures of parallel image processing," in *Proc. Conf. Pattern Recognition in Practice*, L. N. Kanal and E. S. Gelsema, Eds. Amsterdam, The Netherlands: North-Holland, 1980.

[38] ——, "Biomedical image processing," *IEEE Comput. Mag.*, vol. 16, Jan. 1983.

[39] ——, "Gray-scale morphology," *Comput. Graphics Image Processing*, vol. 35, pp. 333–355, 1986.

[40] S. W. Zucker, R. A. Hummel, and A. Rosenfeld, "An application of relaxation labeling to line and curve enhancement," *IEEE Trans. Comput.*, vol. C-26, pp. 394–403, Apr. 1977.

[41] J. F. Brenner, J. M. Lester, and W. D. Selles, "Scene segmentation in automatic histo-pathology: Techniques of Cytology Automation," *Pattern Recognition*, vol. 13, pp. 65–77, 1981.

James S. J. Lee (S'83-M'85) was born in Chang-Hwa, Taiwan, in 1955. He received the B.S. degree in control engineering from National Chiao Tung University in 1977, the M.S. degree in electrical engineering from National Taiwan University in 1979, and the Ph.D. degree from Virginia Polytechnic Institute and State University, Blacksburg, VA, in 1985.

From 1980 to 1981, he was an engineering officer of the Electrical Division in the R.O.C. Navy Third shipbuilding yard for the required ROTC military service. He was awarded the outstanding invention prize by the R.O.C. Navy general headquarters and the "First Prize of Invention" by the R.O.C. Ministry of Education. From 1981 to 1982 he was an Instructor in the Department of Electronic Technology, National Taiwan Institute of Technology. His activities there included teaching and robotics research. From 1982 to 1984, he was a Research Assistant at the Spatial Data Analysis Laboratory of Virginia Tech engaged in image processing and artificial intelligence research. From 1984 to 1986 he was a Research Scientist at the Research and Development Department of Machine Vision International where he conducted research in real-time machine vision algorithm and architecture. In the fall of 1986 he joined the High Technology Center of the Boeing Electronics Company as a Senior Specialist Engineer in the Information Processing Laboratory. His current research interests include adaptive image processing, real-time machine vision architecture, intelligent vision systems, distributed problem solving, machine learning, and sensor fusion.

Dr. Lee is a member of Phi Kappa Phi.

Robert M. Haralick (S'62-S'67-M'69-SM'76-F'84) was born in Brooklyn, NY, on September 30, 1943. He received the B.A. degree in mathematics from the University of Kansas, Lawrence, in 1964, the B.S. degree in electrical engineering in 1966, the M.S. degree in electrical engineering in 1967, and the Ph.D. degree in 1969.

He has worked with Autonetics and IBM. In 1965 he worked for the Center for Research, University of Kansas, as a Research Engineer and in 1969 he joined the faculty of the Electrical Engineering Department where he served as a Professor from 1975 to 1978. In 1979 he joined the faculty of the Electrical Engineering Department at Virginia Polytechnic Institute and State University where he was a Professor and Director of the Spatial Data Analysis Laboratory. From 1984 to 1986 Dr. Haralick served as Vice President of Research at Machine Vision International, Ann Arbor, MI. He now occupies the Boeing chaired professorship in the Department of Electrical Engineering at the University of Washington, Seattle. He has done research in pattern recognition, multimage processing, remote sensing, texture analysis, data compression, clustering, artificial intelligence, and general systems theory. He is responsible for the development of GIPSY (general image processing system), a multimage processing package which runs on a minicomputer system.

Dr. Haralick is a member of the Association for Computer Machinery and the Pattern Recognition Society.

Linda G. Shapiro (S'74-M'74-M'81-SM'81) was born in Chicago, IL, in 1949. She received the B.S. degree in mathematics from the University of Illinois, Urbana, in 1970, and the M.S. and Ph.D. degrees in computer science from the University of Iowa, Iowa City, in 1972 and 1974, respectively.

She was an Assistant Professor of Computer Science at Kansas State University, Manhattan, from 1974 to 1978 and was an Assistant Professor of Computer Science from 1979 to 1981 and Associate Professor of Computer Science from 1981 to 1984 at Virginia Polytechnic Institute and State University, Blacksburg. She was Director of Intelligent Systems at Machine Vision International in Ann Arbor, MI, from 1984 to 1986. She is currently an Associate Professor of Electrical Engineering at the University of Washington, Seattle. Her research interests include computer vision, artificial intelligence, pattern recognition, robotics, and spatial database systems. She has coauthored a textbook on data structures with R. Baron.

Dr. Shapiro is a senior member of the IEEE Computer Society and a member of the Association for Computing Machinery, the Pattern Recognition Society, and the American Association for Artificial Intelligence. She is Editor of *Computer Vision, Graphics, and Image Processing* and an editorial board member of *Pattern Recognition*. She was recently the General Chairman of the IEEE Conference on Computer Vision and Pattern Recognition held in Miami, FL, June 1986.